RSC Advances

ROYAL SOCIETY OF CHEMISTRY

www.rsc.org/advances

Journal Name

RSCPublishing

ARTICLE

Polymeric Cathode Materials of Electroactive Conducting Poly(triphenylamine) with Optimized Structures for Potential Organic Pseudo-capacitors with Higher Cut-off Voltage and Energy Density†

Cite this: DOI: 10.1039/x0xx00000x

Received 00th January 2012,
Accepted 00th January 2012

DOI: 10.1039/x0xx00000x

www.rsc.org/

Wei Ni,[ab] Jianli Cheng,[ab] Xiaodong Li,[ab] Guifang Gu,[ab] Ling Huang,[ab] Qun Guan,[ab] Demao Yuan[ab] and Bin Wang*[ab]

For the electrochemical capacitors or supercapacitors, pseudo-capacitors, *via* the fast surface reactions, are able to storage/harvest more electrical energy compared with electrochemical double layer capacitors (EDLCs) by the ion adsorption route. Combination of pseudo-capacitive materials including oxides, nitrides and polymers, as well as the understanding charge storage mechanisms and the development of advanced nanostructures, with the latest generation of nanostructured lithium electrodes has brought the energy density of electrochemcial capacitors closer to that of batteries. Electroactive polymeric cathodes with designed structures, *via* the electrospinning (without polymeric additives) and surfactant-free precipitation polymerization routes, were herein fabricated for the abovementioned goals. The as-prepared polymeric active materials showed an electrochemical capacitance of around 200 F g^{-1}, with a higher cut-off voltage up to 4.2 V and an energy density up to 370 Wh kg^{-1} and power density up to 34 kW kg^{-1} in an organic electrolyte system.

Introduction

Nanoscale design of the structure and chemistry of electrode materials may enable us to develop a new generation of devices that approach the theoretical limit for electrochemical storage and deliver electrical energy rapid and efficiently.[1, 2] Electrochemical capacitors, also named supercapacitors, store energy using either ion adsorption or fast surface redox reaction (i.e., pseudo-capacitors), which may complement or replace batteries when higher power delivery or undertake is needed in electrical energy storage and harvesting applications. The combination of pseudo-capacitive nanomaterials, including oxides, nitrides and polymers, with the latest generation of nanostructures lithium electrodes has been one of the notable improvements *via* further understanding charge storage mechanisms as well as superior electrode architecture design, which has brought the energy density of electrochemical capacitors closer to that of batteries.[3, 4]

Electroactive conducting polymers (ECPs) are a large family of organic flexible materials capable of high-rate storage and deliver of electric energy because of their high electronic conductivity and feasible rapid electrochemical kinetics,[5, 6] which may be one of the ideal electrical energy storage candidate materials to overcome one of the highly challenging issues due to the kinetic limitations of the pseudo-capacitive electrodes in high energy density asymmetric supercapacitors.[7] Supercapacitors electrodes and devices that utilize conducting polymers are envisaged to bridge the gap between existing carbon-based supercapacitors and batteries to from unites of intermediate specific energy.[8] Conducting polymers are pseudo-capacitive materials, which undergo a fast redox reaction to provide the capacitive response. In the past two decades, various conducting polymers, such as polyaniline,[9] polythiophene,[10] poly(*p*-phenylene) and their derivatives, have been studied as electrode materials for electrochemical energy storage and harvesting applications. Compared with other supercapacitors materials such as carbon or inorganic ones, the bulk of the ECPs materials undergo a fast redox reaction to provide the pseudo-capacitive response and exhibit superior specific energy to the carbon-based double-layer capacitors and more conductive than the inorganic battery materials and consequently possess greater power capability.[8] Amongst the electroactive conductive polymers, polytriphenylamines (PTPA) seem to be a kind of ideal polymers as required to have a highly conductive polyphenylene backbone combined with high energy density of electroactive polyaniline,[11] which may be synthesized by a facile chemical or electrochemical oxidation of their monomers. Compared with an electrochemical route, the chemical oxidation route generally offers a higher degree of polymerization and structural homogeneity for the PTPA production through an excessive oxidant addition.[11, 12] Their hole-transporting abilities are based on the fact that they can be easily oxidized to form stable radical cation, which may be further developed as a kind of cathode material in polymer supercapacitors. Since that the low molecular weight compounds from TPA derivatives (i.e., oligomers), as well as

most electroactive conducting polymers,[13, 14] have some problems such as the lack of thermal stability and/or mechanical strength or difficulty for fabricating such conjugated polymers into required structures due to their rigid molecular skeletons. In order to solve these problems, it is proposed to fabricate flexible materials or highly crosslinked materials to enhance the structural and electrochemical stability. For example, one-dimensional (1D) structures with smaller scale properties may satisfy the related demands for the conjugated conducting polymers, of which the electrospinning is an effective approach to fabricate long polymer fibers with controllable diameters by using strong electrostatic forces. Compared with other synthetic approaches, the electrospinning process seems to be the only method that can mass-produce continuous long thin-fibers and the free-standing networks thereof. [13, 14, 15]

We here present a kind of ECPs, i.e., poly(triphenylamine) microfibers, and particulates comprised of nanofibrils for high-rate and light-weight electrochemical pseudo-capacitors with widened operating voltage widows. Compared with the higher-potential supercapacitors with inorganic electrode materials and organic electrolytes,[7, 16-18] this approach may provide another general strategy for the fabrication of polymer-based supercapacitors with organic or gel polymer electrolytes, i.e., all-organic supercapacitors.[19]

Results and discussion

A representative electrospinning process and the scanning electron microscopy (SEM) images of the PTPA fibers, which were electrospun from its good solvent chloroform (**Figure 1**). The fibers showed an average diameter of *ca.* 10 μm and possessed a large aspect ratio. And at the macro level, the electrospun microfibers exhibited a pale yellow appearance, the fibers were somewhat rigid and no distinct intertwined networks were noticed as that for most one-dimensional polymer nanostructures.[20-22] For the PTPA sample with excessive oxidation reaction, it can be observed from the SEM that the particulates obtained from the precipitation polymerization process revealed a hierarchically porous structure constructed by intertwined nanofibrils (*ca.* 100–200 nm) (**Figure 2**), and the presence of larger pores between the particulates enables rapid electrolyte transport while the smaller pores inside the particulates effectively increase the surface area available for electrochemical reactions between solid-liquid interfaces.[7] The tiny nanofiber and nanoparticle dimensions will allow effective electrolyte anion (e.g. PF_6^-) diffusion. Since the highly-crosslinked PTPA were insoluble in any typical solvents such as DMF (*N*,*N*-Dimethylformamide), NMP (1-Methyl-2-pyrrolidone), chloroform, and electrolyte solvents such as EC (ethylene carbonate), DEC (diethyl carbonate), DMC (dimethyl carbonate) etc., it may perform a better stability for the electrochemical device applications thereof (for the solubility in chloroform as an example, see **Figure S1** in ESI†).

The Fourier transform infrared (FTIR) spectra of two kinds of PTPA, with their monomer TPA as comparison, obtained using compressed KBr pellet technique are shown in **Figure 3**, and the main characteristic IR vibration peaks are marked. The band at 1273 cm^{-1} is assigned to C–N stretching, from tertiary amines, and the band at 817 cm^{-1} is assigned to a C-H out-of-plane vibration from *para*-disubstituted benzene rings,[23] thus the significant bands present at 1273 and 817 cm^{-1} indicate coupling of the starting material, i.e. that C–C bonding between the benzene rings of the triphenylamine units or the chemical polymerization has taken place.[24] The vibrations from C–C stretching at 1489 cm^{-1} and from C–H bending at 1319 can also be observed in the spectrum, which corresponds to the main vibration bands characteristic of the TPA moieties.[11] The quinoid structures associated with the vibrations from C=C stretching (i.e. C–C stretching in quinoid) at 1592 cm^{-1} and from C–H bending at 1109 cm^{-1} revealed in the spectrum indicate that the polymer is not yet charged, or the separation status between the charge carriers and the highly crosslinked structure of the polymer (i.e. fully discharged).[24] The proposed assignments of infrared vibrations are all corresponded to the pristine PTPA, since that upon charging of these kind of conjugated materials, new bands will appear in the IR spectra from 1500 to 700 cm^{-1}, typically named the IR-active vibration bands (IRAV), which are usually 20–30 times stronger in intensity and grow linearly with an increasing concentration of charge carriers.[24] Besides, the PTPA in a particulate morphology almost showed the similar characteristic peaks and peak intensity, which revealed that there had been no precursor, i.e. TPA, remained as residual in the as-prepared two kinds of PTPA and reached a favorable degree of polymerization.

XRD patterns of the product and precursor were obtained by a powder X-ray diffraction and shown in **Figure 4**. As expected, the PTPA samples whether in a fibrous or particulate morphology displayed a non-ordered, amorphous structure determined by the XRD measurements which showed only one main broad peak around $2\theta = 20^o$, compared to that of the precursor TPA monomer with strong crystal diffraction peaks. And no indication of π-stacking was evident at $2\theta = \sim 26^o$ from the related investigations.[25] Besides, the PTPA sample of particulate morphology with higher degree of polymerization (DP) even revealed a weaker diffraction peak compared to that of the fibrous one with lower DP. The as-synthesized materials were thermally stable in nitrogen atmosphere up to 500 ^oC, as revealed by thermal gravimetric analysis (TGA), and the particulate PTPA sample showed a better thermal stability and might be basically attributed to the nature of the much higher cross-linked networks for the molecular skeletons (**Figure 5**).[25] Furthermore, the ^1H NMR data (6.96–7.46 ppm) of the as-synthesized soluble polymer PTPA showed a decreased content of H atoms as compared to the ^1H NMR data (6.98–7.43 ppm) of its monomer TPA, which further confirmed the dehydrogenation polymerization process during the oxidation reaction (**Figure S2** in ESI†).

Generally, the redox cycles of electroactive conducting polymers (ECPs) perform upon an anion insertion/extraction process, i.e., the oxidation *via* an insertion of electrolyte anions (A^-) into the cathode materials, which compensates positive charges in the electrochemically oxidized cathode ECPs, followed by expulsion of the inserted anions to the electrolyte solution upon reduction and the cations return from the counter electrode to restore the electrolyte.[24] These processes are somewhat different from the mechanism of traditional lithium-ion batteries but quite similar to that of supercapacitors, as illustrated in **Scheme 1** (taking PTPA as an example). The electrochemical performances of the PTPA samples were further investigated using two-electrode cells, in which the lithium foil was used as both the counter and reference electrodes. Charge and discharge behaviors were characterized by cyclic voltammetry (CV) and galvanostatic methods. In a charging cycle, the faradaic current starts to increase during *p*-doping. The electrochemical anion PF_6^- insertion process from the organic electrolyte, occurring at cathode PTPA electrodes (for the molecular-level doping mechanism, see **Figure S3** and

S4 in ESI†), can be expressed by the Equation 1, where n is the mole fraction of inserted PF_6^- anions.

$$PTPA + nA^- \leftrightarrow (PTPA)^{n+} nA^- + ne^- \quad \text{(Equation 1)}$$

Since the energy density (E) of a capacitor is governed by $E = 1/2\ CV^2$, where C is the capacitance and V is the cell potential, increasing the potential or capacitance will lead to a higher energy density.[7] Because of the large electrochemical window of the organic electrolytes, a larger cell voltage of 4.2 V, compared with the aqueous supercapacitors,[26, 27] was observed for the PTPA capacitors. As can be seen in **Figure 6A**, the current density of PTPA fiber capacitor increased with a scan rate from 1 to 10 mV s^{-1}, and the peak height was basically proportional to the scan rate, and the integral area or the capacitance calculated kept basically stable, which indicated a fast and effective diffusion of ions for the PTPA electrode. Up on galvanostatic charging/discharging, the PTPA pseudo-capacitor showed an excellent charge storage and delivery performance (**Figure 6B**). The capacitance was calculated by an equation followed,

$$C_m = I \cdot \Delta t / m \cdot \Delta U \quad \text{(Equation 2)}$$

where C_m (F g^{-1}) indicates the specific capacitance, I (A) is the discharge current density, Δt (s) is the discharge time, ΔU (V) represents the potential change during discharge, and m (g) the mass of the active materials in cathode, respectively.[7, 28] And the capacity calculated by the galvanostatic method showed that the PTPA electroactive material possessed a relative high capacity of around 200 F g^{-1}, based on a potential window of 4.2–2.5 V. While for the particulate sample, the capacity decreased with the increasing current density, the cathode active materials showed a discharge capacity in the range of *ca.* 180–100 F g^{-1} with the discharge current density increased from 0.5 mA g^{-1} to 10 mA g^{-1} (**Figure 6C**). The capacity retention ratio for the PTPA fibers were 89.2% after 1000 cycles and 83.5% after 2000 cycles, respectively, with a charge/discharge current density of 2 A g^{-1} (**Figure 6D**).

ECPs-based redox supercapacitors will provide enhanced performance with respect to that of commercial double-layer devices if thick electrodes can be doped without many kinetic problems.[29] To further explore the electrochemical properties and the electroactive transformation, a complete kinetic characterization of the doping process of PTPA, i.e., the electrochemical impedance spectroscopy (EIS) measurements of electrode potentiostatically charged at several potentials were carried out (**Figure 6E**). The impedances at high frequency (100 kHz) reflect the equivalent series resistance (ESR) in the electrode/electrolyte system, which is contributed from both the electrolyte resistance and electronic resistance of the hybrid electrode.[30] For the capacitor made from the PTPA fiber, as the cycling proceeding the electronic resistance of the hybrid electrode decreased from 17.1 to 13.3 Ohm, while the same trend happened with the higher charging potential (e.g., 4.2 V; decreasing to 9.6 Ohm), which could both be attributed to the increasing electric conductance due to the activation or doping effect. The charge-transfer resistance (R_{ct}), which is believed to be one of the important factors in electrochemical reactions and reflected in the diameter of the semicircle along the Z′ axis, revealed a similar decreasing trend (from 254 Ohm to 56, 30 Ohm). On the whole, the capacitive characteristic was observed as a vertical line when the frequency is lower that 100 mHz, and a depressed semi-circle was observed at relatively high frequencies, which might represent a parallel combination of resistive and capacitive components.[31] The EIS data are fitted according to the equivalent in Figure 6E (inset), which contains R_Ω (electrolyte resistance), R_{ct} (charge transfer resistance), R_L (resistance roughly representing the dissipative part of the finite diffusion process of the counterions in the polymers), and Z_w (the Warburg impedance), C_{dl} (the electric double layer capacitance), and C_L (the limit capacitance).[29] The EIS features of ECPs-based pseudocapacitors are somewhat similar to that of transition metals-based pseudocapacitors.[32]

And for demonstrating the operational characteristics, the average power density (P_{av}) may be calculated at different scan rates according to the following Equation,

$$P_{av} = E/t \quad \text{(Equation 3)}$$

where t is indicating the discharge time (s).[33] The Ragone plot of energy density (E) versus power density (P) for the PTPA hybrid electrodes are listed in **Figure 6F**. The E and P values were calculated from galvanostatic discharge curves considering the mass of active material in the cathode (or positive electrode). The maximum energy density of 365 Wh kg^{-1} and the highest power density of 33.6 kW kg^{-1} were achieved for the hybrid electrochemical capacitor based on PTPA microfibers at an operation voltage of 4.2 V, while that of PTPA particulate hybrid electrode showed a bit lower E & P values with an obvious downtrend for energy density with increasing power density (i.e., showing an energy density decline from 314 to 250 Wh kg^{-1} with the power density in the range of 1.83–29.0 kW kg^{-1}). Compared to the traditional Li-ion batteries, this kind of electrochemical capacitor showed a substantially higher power density, and a greatly improved energy density compared to that of the traditional electric double layer capacitors (EDLCs).

Conclusions

In summary, we here described a facile and scalable electrospinning-based approach for the preparation of thin-fibers of the electroactive conducting polymer and the fabrication of high-performance hybrid electrodes for electrochemical capacitors. The polymer-based hybrid electrode structures allow an efficient use of pseudo-capacitive ECPs for charge storage with facilitated transport of both electrolyte ions and electrons, thus rendering the electrode materials with high specific capacitance, superior rate capability and remarkable cycling performance, which are believed to offer great promise in electric vehicle or grid-scale energy storage applications.

Experimental

Materials. Triphenylamine (Aladdin Chemical Reagent Co., China), chloroform (AR, Chengdu Kelong Chemical Reagent Co., China), and $FeCl_3$ (anhydrous, AR, 98.0 %, Shanghai Shanpu Chemical Co., Ltd., China) were used directly with further purification.

Preparation and Structural Characterization of polytriphenylamine. Polytriphenylamine (PTPA) was prepared in a modified chemical oxidative method as reported in literature.[12] As a typical one for highly crosslinked PTPA, 0.25 m (6.13 g) triphenylamine monomer dissolved in 100 mL chloroform was first prepared and 0.025 mol (4.05 g) $FeCl_3$ was added under a nitrogen atmosphere, followed by intense magnetic stirring. The remaining $FeCl_3$ oxidant was subsequently added into the reaction solution at an interval of 1 h, with total amount of $FeCl_3$ used four times of TPA. The oxidative polymerization of TPA usually takes two more hours

in the solution under nitrogen atmosphere. After the solution polymerization reaction completed, the reaction mixture was poured into methanol to deposit the polymer product, which was filtered and washed with methanol and chloroform several times for purification. Finally, the polymer product was dried in vacuum at 50 °C overnight. As another typical one for lower molecular weight PTPA, the $FeCl_3$ oxidant was only added twice, i.e. the total amount used was two times of TPA, and the oxidative polymerization process took about two hours. The other conditions and procedures were kept the same as above mentioned.

Polytriphenylamine solution with a concentration of *ca.* 20 wt.% in chloroform was used for electrospinning process. A piece of grounded aluminum foil was placed 20 cm below the single-nozzle spinneret to collect the fibers. A high voltage of 20 kV was supplied at the spinneret by a direct-current power supply, and the typical feeding rate was set at *ca.* 100 μL min^{-1}. The electrospun PTPA microfibers were collected at room temperature in air atmosphere and dried in vacuum for further use.

The morphology was investigated using a scanning electron microscope (SEM, TESCAN VEGA3) operating at 15 kV after Pt coating. The crystal structure of the samples was obtained by X-ray diffraction analysis (XRD, PANalytical X'Pert Pro, Cu Kα radiation, λ = 1.5418 Å) over a 2θ range of 5–80°. The thermal decomposition process and thermal analysis were conducted on a thermogravimetric analyzer (TGA/DSC 1, Mettler Toledo) with a heating rate of 10 °C min^{-1} between 50 and 1000 °C. FTIR spectra were taken on a Nicolet Magna IR-560 spectrometer. ^{1}H NMR and ^{13}C NMR spectra were recorded on Bruker AVANCE II 400 MHz spectrometer, with tetramethylsilane (TMS) as internal standard and $CDCl_3$ as solvent.

Electrode Fabrication and Electrochemical Measurements. The PTPA fibers, or highly crosslinked porous particulates were assembled onto copper foil current collectors. Briefly, 70% of the electrochemically active material PTPA, 20% carbon black, and 10% poly(vinylidene fluoride) (PVDF) dispersed in *N*-methylpyrrolidinone (NMP) were mixed and magnetically stirred to form slurries. The homogenous slurry was coated on a copper foil substrate and dried at 80 °C over night under vacuum. Electrodes of 12 mm in diameter were assembled into coin-type cells (CR2032) in an argon-filled glove box. The electrolyte solution was 1 m $LiPF_6$ in EC/DEC (ethylene carbonate/diethyl carbonate, v/v = 1/1) solution and lithium foils were used as both the counter and reference electrodes. The separator is constituted by glass fiber (GF/D) membrane (Whatman) soaked with electrolyte. Cyclic voltammetry (CV) measurements were made with a Bio-Logic VSP Electrochemical Workstation (BioLogic Science Instruments, France), using cut-off voltages of 4.2–2.5 V versus Li/Li^+. The galvanostatic charge-discharge experiments were carried out on a LAND CT2001A testing system (Wuhan LAND Electronics Co., Ltd., China) at varied current densities.

Acknowledgements

This work is supported by the Startup Foundation of China Academy of Engineering Physics, Institute of Chemical Materials (KJCX201301 and KJCX201306) and Science and Technology Planning Project of Sichuan Province, China (2014JY0202). One of the authors (W.N.) appreciates the assistance of Mr. Hang Li for FTIR and NMR characterization at College of Polymer Science and Engineering, Sichuan University.

Notes and references

[a] *Institute of Chemical Materials, China Academy of Engineering Physics, Mianyang 621900, China. E-mail: edward.bwang@gmail.com, binwang@caep.cn; Fax: +86 816-2544426*
[b] *Sichuan Research Center of New Materials, Mianyang 621000, China*

† Electronic Supplementary Information (ESI) available: NMR characterization data and the structural formula of as-synthesized polymers and the doping features. See DOI: 10.1039/b000000x/

1. Y. Gogotsi, *ACS nano*, 2014, **8**, 5369-5371.
2. J. Jiang, Y. Li, J. Liu, X. Huang, C. Yuan and X. W. Lou, *Adv. Mater.*, 2012, **24**, 5166-5180.
3. P. Simon and Y. Gogotsi, *Nat. Mater.*, 2008, **7**, 845-854.
4. G. Yu, X. Xie, L. Pan, Z. Bao and Y. Cui, *Nano Energy*, 2013, **2**, 213-234.
5. G. G. Wallace, P. R. Teasdale, G. M. Spinks and L. A. Kane-Maguire, *Conductive electroactive polymers: intelligent polymer systems*, CRC press, 2008.
6. G. Inzelt, *Conducting polymers*, Springer, 2008.
7. Z. Chen, V. Augustyn, J. Wen, Y. Zhang, M. Shen, B. Dunn and Y. Lu, *Adv. Mater.*, 2011, **23**, 791-795.
8. G. A. Snook, P. Kao and A. S. Best, *J. Power Sources*, 2011, **196**, 1-12.
9. K. Zhang, L. L. Zhang, X. S. Zhao and J. Wu, *Chem. Mater.*, **22**, 1392-1401.
10. A. Laforgue, P. Simon, C. Sarrazin and J.-F. Fauvarque, *J. power sources*, 1999, **80**, 142-148.
11. J. Feng, Y. Cao, X. Ai and H. Yang, *J. power sources*, 2008, **177**, 199-204.
12. C. Takahashi, S. Moriya, N. Fugono, H. C. Lee and H. Sato, *Synth. Met.*, 2002, **129**, 123-128.
13. Z.-M. Huang, Y.-Z. Zhang, M. Kotaki and S. Ramakrishna, *Compos. Sci. Technol.*, 2003, **63**, 2223-2253.
14. Y.-Z. Long, M.-M. Li, C. Gu, M. Wan, J.-L. Duvail, Z. Liu and Z. Fan, *Prog. Polym. Sci.*, 2011, **36**, 1415-1442.
15. P. T. Mather and G. A. Sotzing, U.S. Patent No. 8,178,629, 15 May 2012.
16. D. Wei, M. R. Scherer, C. Bower, P. Andrew, T. Ryhänen and U. Steiner, *Nano Lett.*, 2012, **12**, 1857-1862.
17. D. Y. Liu and J. R. Reynolds, *ACS Appl. Mater. Interfaces*, 2010, **2**, 3586-3593.
18. X. Yang, F. Zhang, L. Zhang, T. Zhang, Y. Huang and Y. Chen, *Adv. Funct. Mater.*, 2013, **23**, 3353-3360.
19. F. Meng and Y. Ding, *Adv. Mater.*, 2011, **23**, 4098-4102.
20. Z. Yin and Q. Zheng, *Adv. Energy Mater.*, 2012, **2**, 179-218.
21. L. Persano, A. Camposeo, C. Tekmen and D. Pisignano, *Macromol. Mater. Eng.*, 2013, **298**, 504-520.
22. W. Teo and S. Ramakrishna, *Nanotechnology*, 2006, **17**, R89.
23. S. Tanaka, K. Takeuchi, M. Asai, T. Iso and M. Ueda, *Synth. Met.*, 2001, **119**, 139-140.
24. C. Kvarnström, A. Petr, P. Damlin, T. Lindfors, A. Ivaska and L. Dunsch, *J. Solid State Electrochem.*, 2002, **6**, 505-512.
25. Y. Liao, J. Weber and C. F. J. Faul, *Chem. Commun.*, 2014, **50**, 8002-8005.

26. P. Si, S. Ding, X.-W. D. Lou and D.-H. Kim, *RSC Adv.*, 2011, **1**, 1271-1278.
27. Q. Guan, J. Cheng, B. Wang, W. Ni, G. Gu, X. Li, L. Huang, G. Yang and F. Nie, *ACS Appl. Mater. Interfaces*, 2014.
28. W. Ni, B. Wang, J. Cheng, X. Li, Q. Guan, G. Gu and L. Huang, *Nanoscale*, 2014, **6**, 2618-2623.
29. C. Arbizzani, M. Catellani, M. Mastragostino and C. Mingazzini, *Electrochim. Acta*, 1995, **40**, 1871-1876.
30. G. Yu, L. Hu, N. Liu, H. Wang, M. Vosgueritchian, Y. Yang, Y. Cui and Z. Bao, *Nano Lett.*, 2011, **11**, 4438-4442.
31. Y.-Z. Wei, B. Fang, S. Iwasa and M. Kumagai, *J. Power Sources*, 2005, **141**, 386-391.
32. X. Wang, X. Han, M. Lim, N. Singh, C. L. Gan, M. Jan and P. S. Lee, *J. Phys. Chem. C*, 2012, **116**, 12448-12454.
33. Z. Fan, J. Yan, T. Wei, L. Zhi, G. Ning, T. Li and F. Wei, *Adv. Funct. Mater.*, 2011, **21**, 2366-2375.

Journal Name RSCPublishing

ARTICLE

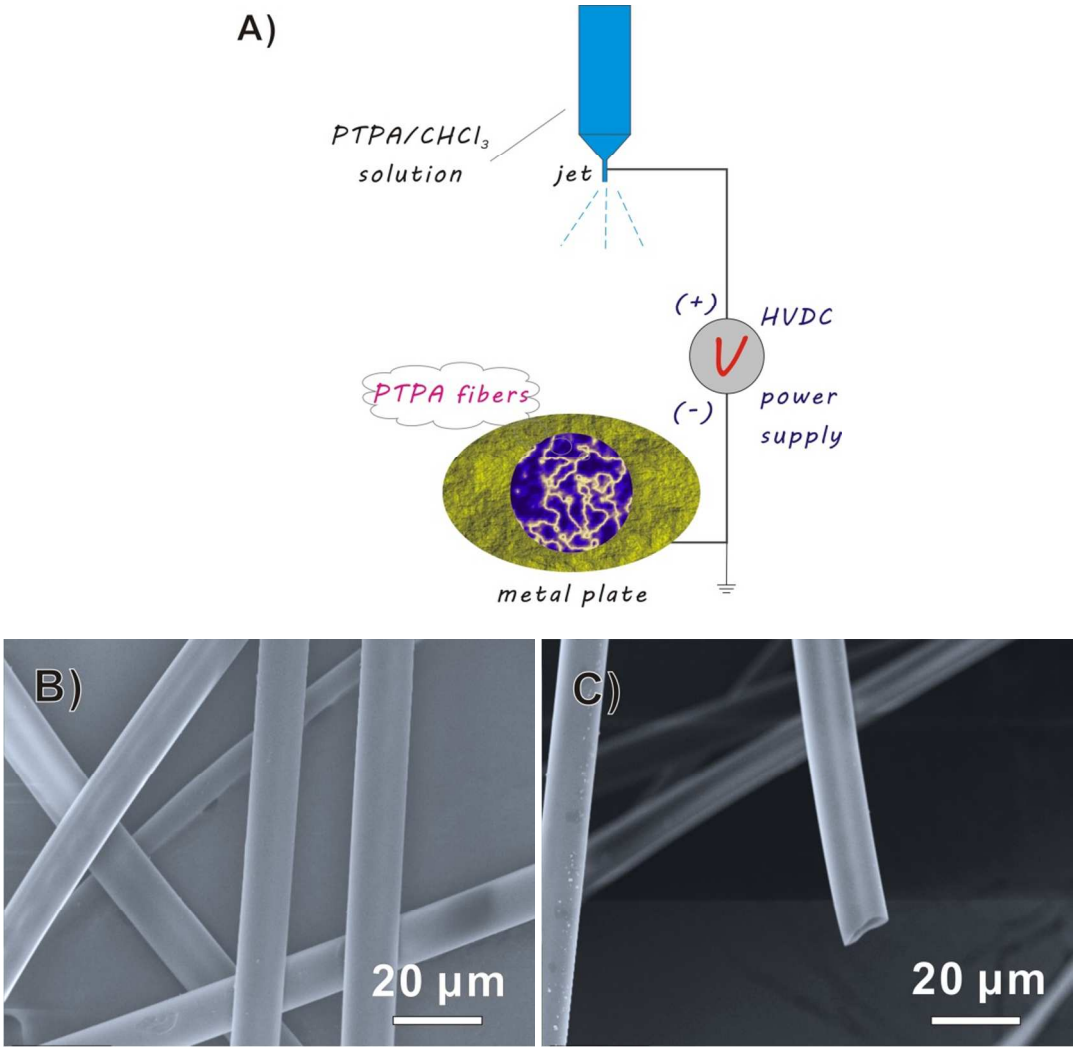

Figure 1. a) Illustration of the direct electrospinning process for PTPA fibers, and b,c) SEM images of the representative electrospun PTPA microfibers.

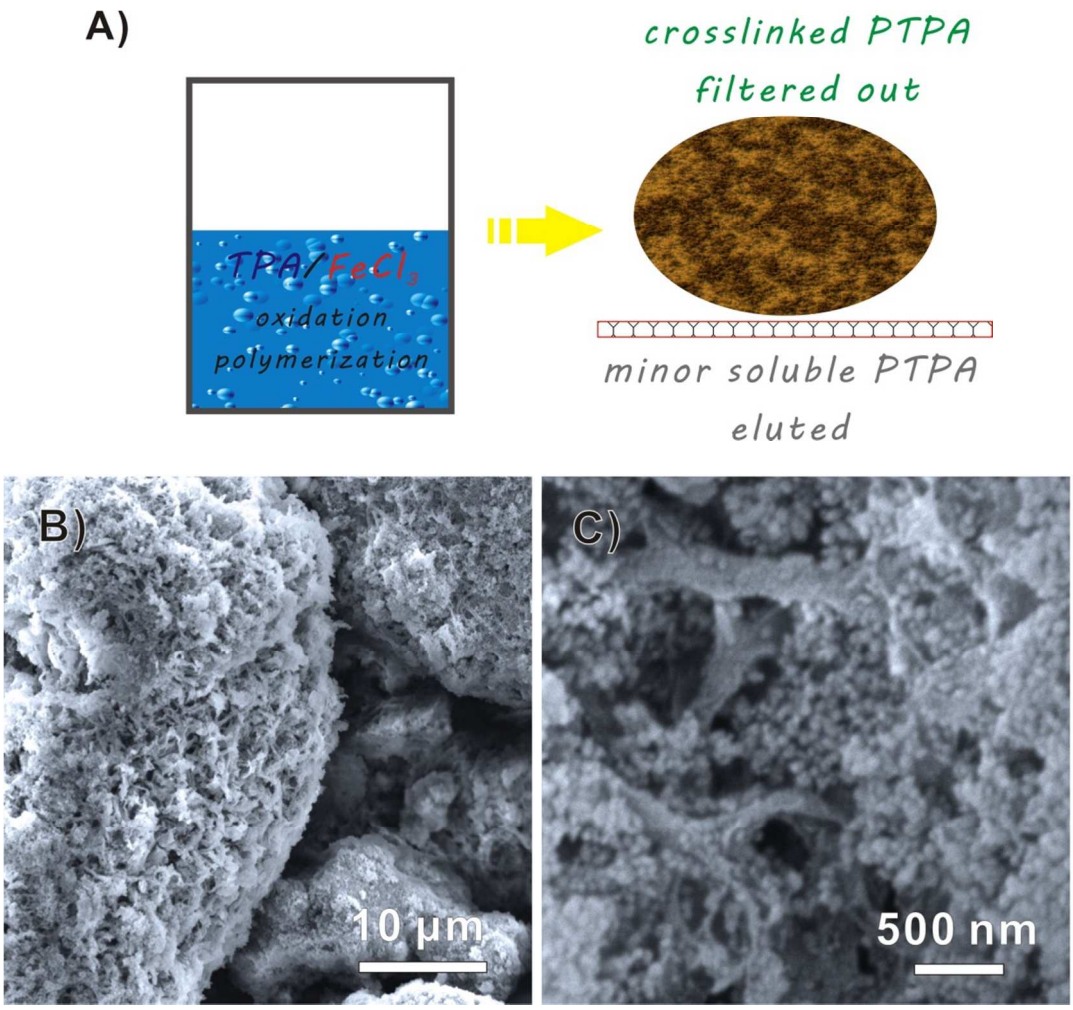

Figure 2. a) Illustration of the oxidation polymerization and collection process for the crosslinked PTPA particulates, and b,c) SEM images of the typical structure of the porous PTPA particulates comprised of nanofibrils, which is insoluble in solvents.

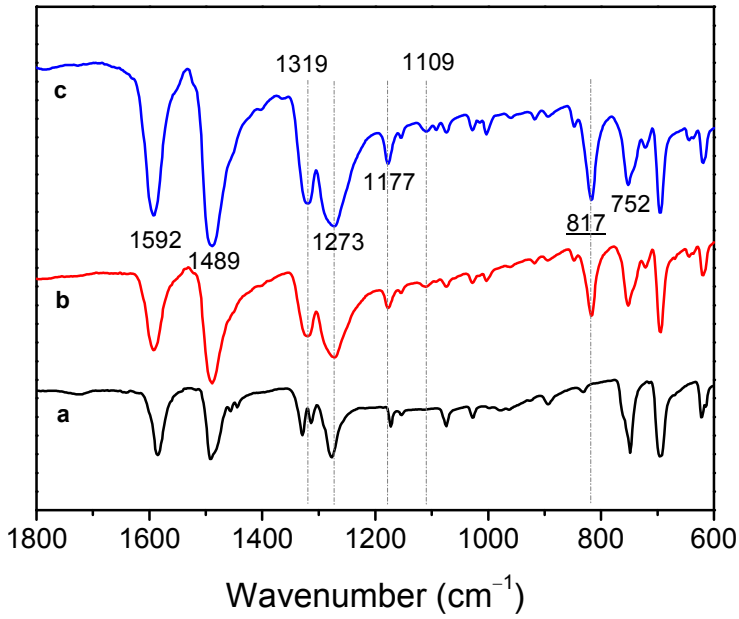

Figure 3. FT-IR spectra of the precursor and as-prepared PTPA samples. a) TPA monomer, b) PTPA fibers, and c) PTPA particulates.

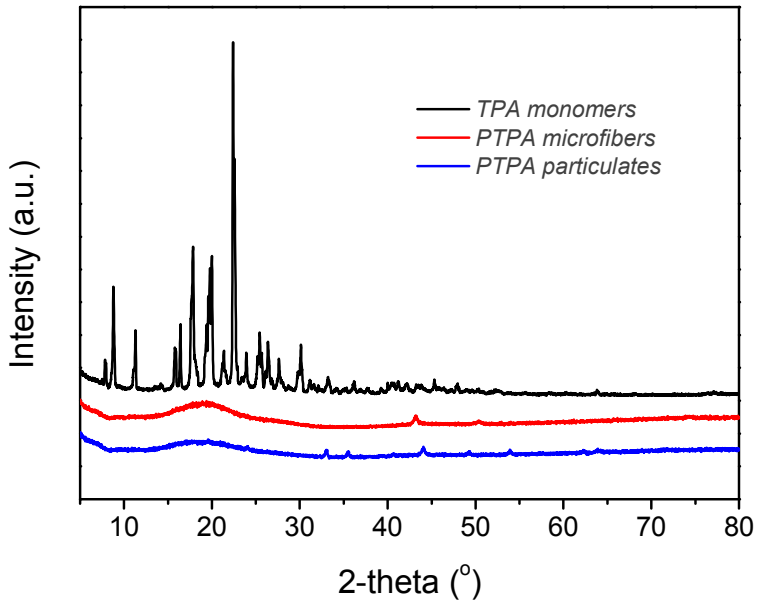

Figure 4. XRD spectra of the TPA monomer (black line), and as-synthesized PTPA microfibers (red line) and PTPA particulates (blue line).

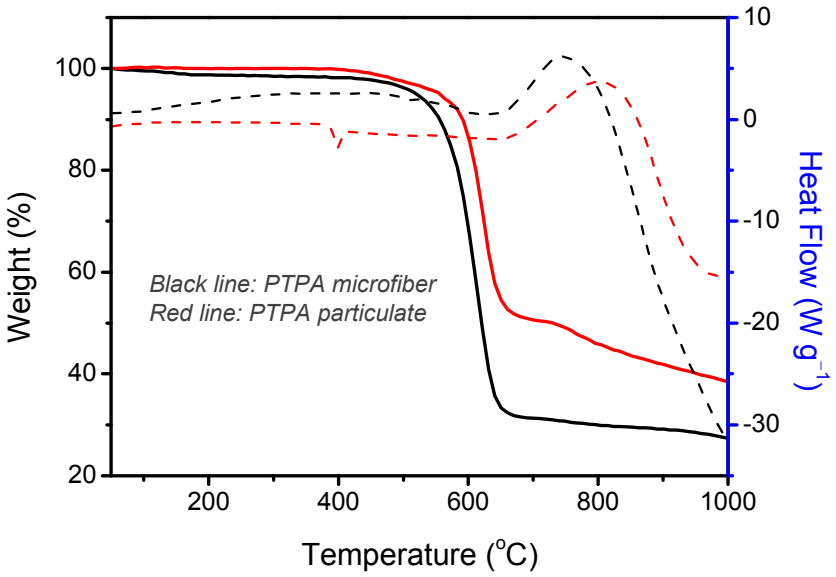

Figure 5. TGA-DSC curves of the as-prepared PTPA samples in nitrogen atmosphere. The corresponding temperature of maximum decomposition is 612 ^{o}C, and 622 ^{o}C for the PTPA microfibers and particulates, respectively.

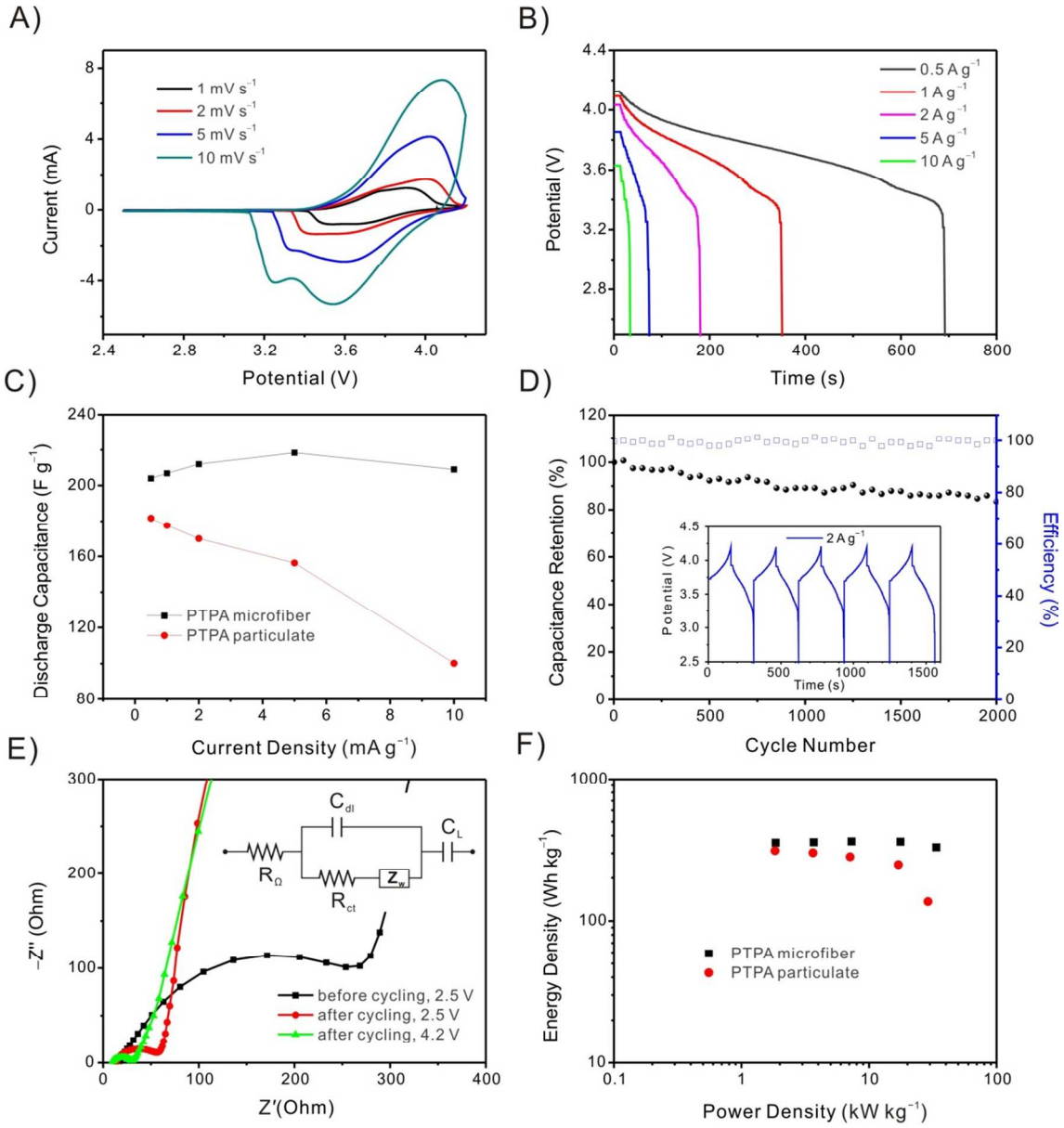

Figure 6. Pseudo-capacitive performances based on PTPA samples. a) CV curves of different scanning rates and b) galvanostatic discharge curves at different current densities with cut-off voltages of 4.2/2.5 V for the PTPA microfibers. c) Specific capacitance at various current rates for the PTPA microfibers and particulates. d) Cycling performance and Coulombic efficiency at a current density of 2 A g^{-1} for the PTPA microfiber electrode, and the inset shows voltage profiles of the typical charge/discharge cycles. e) Nyquist plots of the PTPA microfiber-based electrode. Z′ is real impedance and Z″ is imaginary impedance. Inset: a modified Randles circuit. f) Ragone plots of PTPA capacitor based on microfibers and particulates morphology. Performances of the capacitors are based on the mass of the active electrode materials.

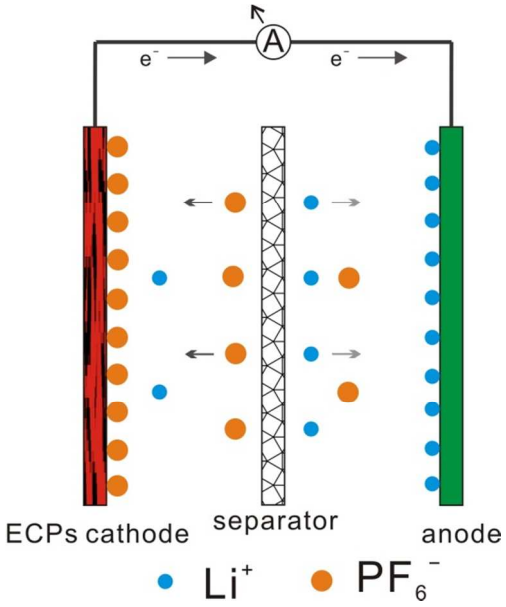

Scheme 1. The illustration of electroactive conducting polymers (ECPs) as cathode (positive electrode) materials for organic-electrolyte-type supercapacitor with $LiPF_6$ as an example. The Faradaic current starts to increase during *p*-doping, i.e., charging process, together with the PF_6^- ions transporting to the cathode and Li^+ to the anode, and followed by a combination of the +/− ions into the electrolyte during a discharging process to complete an electrochemical reaction cycling.

Journal Name RSCPublishing

ARTICLE

Graphical Abstract

Electroactive conducting polymers (ECPs) with designed structures, *via* the fast surface reactions, are able to storage/harvest more electrical energy, which may serve as potential cathode materials of organic pseudo-capacitors with higher voltages.